



ACADÉMIE
DES SCIENCES
INSTITUT DE FRANCE

Comptes Rendus

Géoscience

Sciences de la Planète


Jérôme Aubry, Laurent Bollinger, Alexandre Schubnel, Damien Deldicque
and Jérôme Fortin

Compaction and pore-collapse of chalky limestones from Mururoa atoll

Volume 356 (2024), p. 97-115

Online since: 1 August 2024

<https://doi.org/10.5802/crgeos.266>

 This article is licensed under the
CREATIVE COMMONS ATTRIBUTION 4.0 INTERNATIONAL LICENSE.
<http://creativecommons.org/licenses/by/4.0/>



*The Comptes Rendus. Géoscience — Sciences de la Planète are a member of the
Mersenne Center for open scientific publishing*
www.centre-mersenne.org — e-ISSN : 1778-7025



Research article

Compaction and pore-collapse of chalky limestones from Mururoa atoll

Jérôme Aubry^{*,a}, Laurent Bollinger^a, Alexandre Schubnel^b, Damien Deldicque^b and Jérôme Fortin^b

^a Département Analyse Surveillance Environnement, CEA, DAM, DIF, 91297 Arpajon, France

^b Laboratoire de Géologie, École Normale Supérieure, CNRS, PSL University, 24 Rue Lhomond, 75005 Paris, France

Current address: ISTerre, Université Savoie Mont Blanc, Campus Scientifique, 73376 Le Bourget-du-Lac, France (J. Aubry)

E-mails: jerome.aubry@univ-smb.fr (J. Aubry), laurent.bollinger@cea.fr (L. Bollinger), alexandre.schubnel@ens.fr (A. Schubnel), damien.deldicque@ens.fr (D. Deldicque), jerome.fortin@ens.fr (J. Fortin)

Abstract. Between 1975 and 1996, the Centre d'Expérimentation du Pacifique (CEP) carried out French underground nuclear tests under the atoll of Mururoa (French Polynesia). The deformation of its coral rim was extensively monitored in order to assess the stability of the outer slopes, in particular since a flank collapsed in 1979, triggering a landslide-generated tsunami. The atoll has attracted the attention of experts since the beginning of the nuclear tests because of the mechanical behavior of porous and weak chalky limestones at depth. In this study, samples of these rocks, which were extracted from the atoll's rim through drilling, have been deformed in the laboratory. The implications of the experiments provide a new perspective on the deformation of the Mururoa atoll since the end of nuclear tests—and, by extension, on the micromechanics of chalks for several other geological contexts.

Keywords. Mururoa, Atoll, Chalk, Compaction.

Funding. The LRC Yves Rocard (Laboratoire de Recherche Conventionné CEA-ENS-CNRS).

Manuscript received 11 January 2024, revised 6 May 2024 and 3 June 2024, accepted 4 June 2024.

Key points

- Mururoa's chalky limestones collapse at 16–18 MPa of effective pressure.
- Brittle faulting of chalky limestone can occur below 6 MPa of effective pressure.
- The resistance of chalky limestones is lowered under water saturation.
- Under deviatoric stress, increasing brittle hardening and shear-enhanced compaction are promoted with increasing effective pressure, either in wet or dry conditions.

*Corresponding author

1. Introduction

The deformation of chalks can have significant impacts on the mechanical instability of underground mines and reservoirs [Al Heib et al., 2015, De Gennaro et al., 2004, Georgieva et al., 2020, Geremia et al., 2021, Keszthelyi et al., 2016, Renaud et al., 2019, Risnes et al., 1994, Sulak, 1991]. This deformation can sometimes lead to rock collapse, as for coastal cliffs [Brossard and Duperret, 2004, Duperret et al., 2002, 2004, El Khattabi et al., 2018, Mortimore et al., 2004, Senfaute et al., 2009] and submarine slopes, that could induce tsunamigenic waves [e.g. Abadie et al., 2012, McGuire, 2006, McMurtry et al., 2004, Ward and Day, 2001, Wright and Rathje,

2003]. Slope instabilities are frequent on volcanic islands [Rowberry *et al.*, 2023] but remain under-documented on atolls.

An atoll is a ring-shaped coral reef island, usually surrounding a central lagoon. Most of the world's atolls are in the Pacific Ocean. This is the case of Mururoa Atoll (French Polynesia, France; Figure 1a), an atoll famous as the site of the Centre d'Expérimentation du Pacifique (CEP). 147 underground nuclear tests were carried out there between 1975 and 1996. One of these nuclear tests (*Tydée*) was followed by a submarine flank collapse and a tsunami generated at the Southwest rim of the atoll in 1979 [Poupardin *et al.*, 2017; Figure 1a].

After *Tydée*, the Military Applications Division of the French Alternative Energies and Atomic Energy Commission (CEA-DAM, Bruyères-le-Châtel, France) set up several generations of systems to monitor the mechanical stability of Mururoa and the safety of neighboring atolls. The monitoring devices included topographic networks (presently composed of continuous GPS, supplemented by frequently measured reference points), seismic stations, tiltmeters, extensometers and trigger alarms. The atoll coral rim is divided morpho-geologically into several regions: an emerged zone, which is distinguished from the inner platform (towards the lagoon, with knolls on the surface) and the outer coral rim (open to the ocean, built on the 12-million-year-old volcano) which includes the reef platform, the algal ridge and the outer slope of the atoll [Buigues *et al.*, 1992, Perrin, 1990; Figure 1b].

The International Society for Rock Mechanics recommended 20 years of monitoring after the last nuclear tests in 1996 [Fairhurst *et al.*, 1999]. In 2016, CEA-DAM decided to continue to monitor the atoll. Instruments that had become obsolete were replaced. New boreholes were drilled in order to instrument the northeastern rim of the atoll, including lateral inclined boreholes for extensometers, and vertical boreholes to monitor the stress/strain heterogeneities with tiltmeters and seismic stations at depth. A 608 m-long core, GEO7D, was drilled and collected, complementing an older core (FG5) sampled earlier in the vicinity. These cores document the entire sedimentary sequence down to the volcanic rocks sequence, which were reached at a mean depth of 600 m, and complement previous core drilling dating back from the 1980's. Succinctly, the

cores displayed carbonates lithologies that lay on volcanic rocks. In carbonates, some porous rocks, called chalky limestones, were affected by an intense deformation. The behavior of this lithological unit is suspected to be related with the displacement of the northeastern flank of the atoll that has reached 2 m locally. The displacement rate has progressively decreased over time [CEA/DAM, 2021]. In order to gain an understanding of the long-term mechanical behavior of chalky limestones sampled in the atoll's rim, we conducted experiments in a laboratory setting.

Compaction experiments are generally performed under hydrostatic or triaxial loading. In the hydrostatic case, grain crushing and pore collapse occur at a critical stress P^* at the onset of inelastic compaction, whether localized or distributed [Duba *et al.*, 1974, Dunn *et al.*, 1973, Fortin *et al.*, 2007, Schock *et al.*, 1973, Wong *et al.*, 1992, 2001, 2004, Wong and Baud, 2012, Zaman *et al.*, 1994, Zhang *et al.*, 1990]. Under triaxial loading and confining pressure, the onset of compaction and crack closure (C') is followed by a transition towards strain hardening at a critical stress C^* during which shear-enhanced compaction occur. In carbonates and porous limestones, dilatancy, microcracking and shear localization occur at low confining pressure while strain-hardening and inelastic (shear-enhanced) compaction, accommodated by crystal plasticity or dilatancy, generally occur at high confining pressure [Baud *et al.*, 2004, 2009, 2017a,b, Fortin *et al.*, 2005, 2009, Menéndez *et al.*, 1996, Nicolas *et al.*, 2016, 2017, Tembe *et al.*, 2008, Vajdova *et al.*, 2004, Wong and Baud, 1999, Wong *et al.*, 2001, Zhang *et al.*, 1990, Zhu *et al.*, 2010]. In both experimental conditions, bulk volume change can be estimated with strain gages in dry conditions [Duba *et al.*, 1974, Schock *et al.*, 1973] or estimated from a pore volume change in water-saturated conditions [Zhang *et al.*, 1990].

Bouchez *et al.* [1997] previously studied and deformed chalky limestones from Mururoa in the laboratory. In their experiments, chalky limestones were compacted in dry conditions at confining pressures of 1.5 and 3 MPa—at higher analogue depth compared to the depth of chalky limestone in nature. Their experiments showed that chalky limestones crept up to 8% of axial deformation. However, Mururoa is a water-saturated atoll, subdivided into gradual fracture zones between the outer slope and the lagoon, with stagnant water with a residence

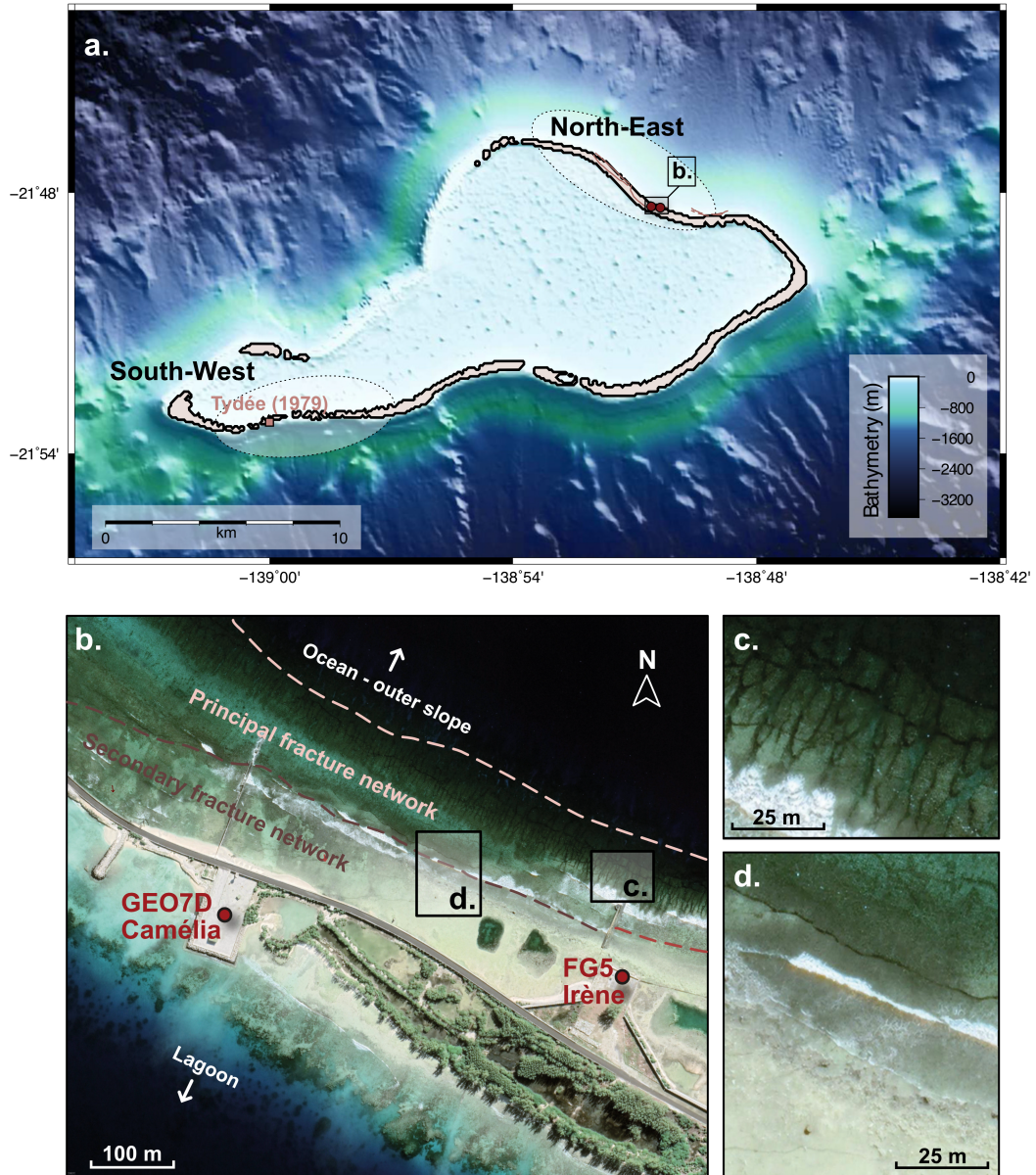


Figure 1. (a) Bathymetry and location of the atoll of Mururoa and (b) close-up view of the north-east area with the main fracture networks (c) and (d).

time greater than 100 days in the central part of the atoll [CEA/DAM, 2021]. Knowing that water-weakening has been observed in porous rocks including chalks [Baud *et al.*, 2009, 2017a,b, Castagna *et al.*, 2018, Lisabeth and Zhu, 2015, Nicolas *et al.*, 2016, 2017], the study of the micromechanics of compaction and deformation of water-saturated chalky limestones seems crucial, although not yet explored.

In this study, (i) we document the intrinsic and mechanical properties of the main lithologies sampled in the two cores forementioned, (ii) we present laboratory experimental results on chalky limestones obtained in various conditions and (iii) draw their mechanical yield envelope. The results provide information on the mechanical deformation of the Mururoa atoll, 28 years after the last French nuclear test,

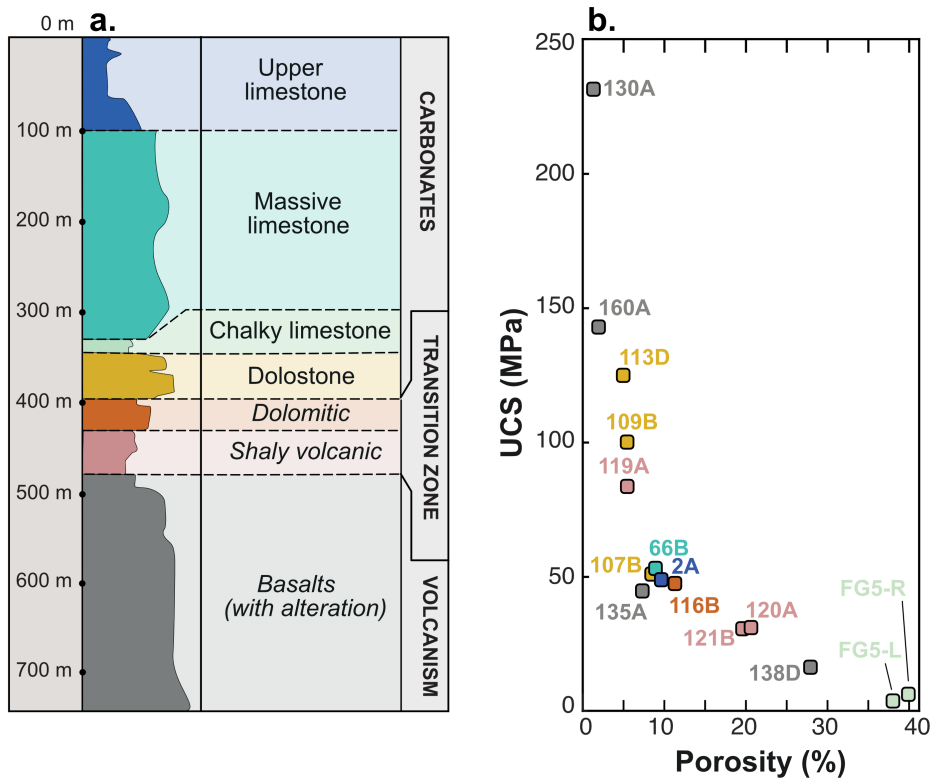


Figure 2. (a) Lithostratigraphic sequence [modified from Buigues et al., 1992] and (b) peak mechanical strength of Mururoa's rocks revealed by uniaxial compressive strength (UCS) as a function of porosity.

offering new insights into the micromechanics of chalk-content rocks in dry and saturated conditions.

2. Methods

2.1. Geological context of the borehole's cores made available

For this study, we used two borehole's cores. The sedimentary rocks sampled in the GEO7D core are similar to those of an older core (FG5) sampled 480 m to the east. The two cores help to document lateral variations in the sedimentary rocks that are open to the ocean (Figure 2a). These rocks consist of a set of carbonates, altered sedimento-volcanic and volcanic facies. The upper facies consists of non-cohesive limestones, interbedded with sandstone-sandy units. These limestones are locally affected by surface cracks and fractures along the northeastern rim of Mururoa atoll—between the algal ridge and the emergent zone—(Figure 1c,d), as in the Takapoto

Atoll [French Polynesia; Montaggioni, 2005]. The lower facies consists of massive limestones, alternating with highly consolidated dolomites, which are in contact with chalky limestones. Downwards, the base of the carbonate facies is composed of indurated and highly heterogeneous dolomites, followed by a dolomitic transition zone that develops in an argilo-volcanic altered geological complex. The transition zone rests on a volcanic base made up of massive basalts, intercalated with more clayey or vacuolated altered volcanic rocks up to 600 m deep on average. Only chalky limestones were sampled in the FG5 core.

2.2. Intrinsic properties collected prior to the laboratory experiments

A preliminary study on the intrinsic properties of representative lithologies of the borehole's cores was carried out prior to the experiments. This

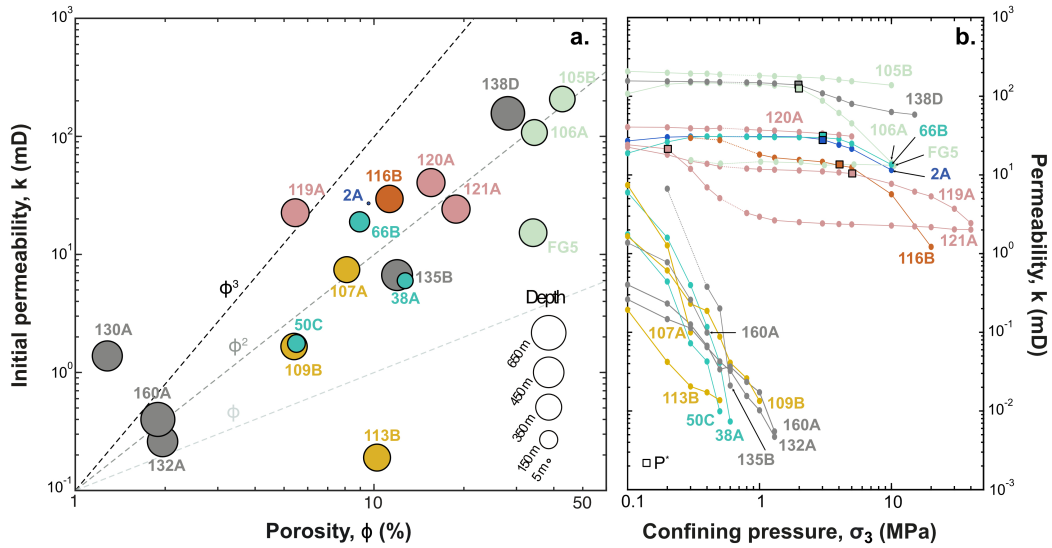


Figure 3. (a) Initial permeability at 0.1 MPa as a function of porosity (color code of Figure 2). (b) Permeability as a function of confining pressure. Permeability is given in mD ($1 \text{ mD} = 10^{-15} \text{ m}^2$).

methodological study helped to locate the chalky limestones within the stratigraphic pile and to understand their differentiated properties compared to other lithologies. Representative samples were selected for uniaxial compressive strength (UCS) tests (Figure 2b). Data on the dry bulk density and the connected porosity ϕ (calculated using the triple-weight method) are shown in Table 1 for several lithologies (Figure 3a). Permeability (symbolized by k) was measured with a gas permeameter (hydrostatic core holder with gas as confining fluid, Top Industrie, Laboratoire de Géologie de l'École Normale Supérieure, Paris, France) between 0.1 and 40 MPa (Figure 3b; Table 2). Pore throat diameter and size distribution of chalky limestones (Figure 4; Table 3) were obtained using a mercury porosimeter (Epitopos, Strasbourg, France).

2.3. Why chalky limestones have been chosen for compaction experiments compared to other lithologies: a singularity revealed by...

2.3.1. A (critical) weakness revealed by uniaxial compressive strength tests

UCS experiments were conducted on dry samples of 40 mm in diameter and 80 mm in length to constrain the intrinsic strength of Mururoa's rocks, in the

absence of confining pressure (Figure 2b, Table 1). The volcano-basaltic bedrock and the dolostones are amongst the most resistant rocks in the sequence, in contrast to the chalky limestones (FG5-R and FG5-L), which appear to be the weakest rocks by far. The UCS experiments provide strong support to target this lithology for the experimental investigation described below.

2.3.2. Very specific intrinsic properties (dry bulk density, permeability, connected and open porosities)

Chalky limestones are found as the most porous rocks in Mururoa: these properties are unique with regard to the other rocks of the lithostratigraphic sequence (except for basaltic sample 138D which is found as porous as chalky limestones; see Figure 3a). The dry bulk densities of chalky limestones are in the range of 1.4–1.6. Their connected porosities are measured between 28 and 54%. In details, chalky limestones are found in a very porous form (connected porosity greater than 35–45%, sample 104A) or a slightly more consolidated form (connected porosity less than 30%, sample 105E). At 0.1 MPa, their initial permeabilities are in the range 10^1 – 10^2 mD ($1 \text{ mD} = 10^{-15} \text{ m}^2$). The permeability of chalky limestones appears to exhibit a strong correlation with a power law in ϕ^2 .

Table 1. Summary of intrinsic properties (density, porosity ϕ and permeability k at 0.1 MPa) and mechanical parameters (critical pore collapse pressure P^* , yield stress at the onset of compaction and of failure) for the samples of the boreholes GEO7D and FG5

Borehole reference	Lithology	Depth (m)	Density	Porosity ϕ (%)	Permeability k at 0.1 MPa (mD)	UCS (MPa)	P^* (MPa)
GEO7D-2A	UPPER LIMESTONE	5.5	2.08	9.59	27.06	48.95	-
GEO7D-2B	UPPER LIMESTONE	5.5	2.39	15.13		-	-
GEO7D-22A	UPPER LIMESTONE	79.4	2.42	7.97		-	-
GEO7D-23A	UPPER LIMESTONE	82.4	2.6	28.63		-	-
GEO7D-31A	UPPER LIMESTONE	113.3	2.71	7.48		-	-
GEO7D-31B	UPPER LIMESTONE	113.3	2.57	6.86		-	-
GEO7D-31D	UPPER LIMESTONE	113.3	2.46	10.72		-	-
GEO7D-35A	MASSIVE LIMESTONE	124.5	2.4	25.17		-	-
GEO7D-35B	MASSIVE LIMESTONE	124.5	2.3	27.25		-	-
GEO7D-38A	MASSIVE LIMESTONE	133.3	2.64	12.72	5.99	-	-
GEO7D-38B	MASSIVE LIMESTONE	133.3	2.58	18.95		-	-
GEO7D-50A	MASSIVE LIMESTONE	166.8	2.42	7.55		-	-
GEO7D-50B	MASSIVE LIMESTONE	166.8	2.51	4.6		-	-
GEO7D-50C	MASSIVE LIMESTONE	166.8	2.5	5.5	1.76	-	-
GEO7D-66A	MASSIVE LIMESTONE	214.4	2.48	12.46		-	-
GEO7D-66B	MASSIVE LIMESTONE	214.4	2.48	8.95	18.89	52.35	-
GEO7D-66C	MASSIVE LIMESTONE	214.4	2.46	14.27		-	-
GEO7D-104A	CHALKY LIMESTONE	338.5	2.22	48.24		-	-
GEO7D-105A	CHALKY LIMESTONE	343.8	2.39	31.59		-	-
GEO7D-105B	CHALKY LIMESTONE	343.8	2.34	42.71	207.21	-	16
GEO7D-105C	CHALKY LIMESTONE	343.8	2.32	37.84		-	18
GEO7D-105D	CHALKY LIMESTONE	343.8	2.39	32.51		-	-
GEO7D-105E	CHALKY LIMESTONE	343.8	2.4	26.4		-	18
GEO7D-105F	CHALKY LIMESTONE	343.8	2.23	40.85		-	-
GEO7D-106A	CHALKY LIMESTONE	360	2.3	36.5	107.8	-	-
FG5-B	CHALKY LIMESTONE	482.5	2.3	40		-	14
FG5-C	CHALKY LIMESTONE	482.5	-	-	-	-	-
FG5-D	CHALKY LIMESTONE	482.5	-	-	-	-	-
FG5-E	CHALKY LIMESTONE	482.5	2.3	35	18.92	-	-
FG5-F	CHALKY LIMESTONE	482.5	-	-	-	-	-
FG5-G	CHALKY LIMESTONE	482.5	-	-	-	-	-
FG5-H	CHALKY LIMESTONE	482.5	-	-	-	-	-
FG5-I	CHALKY LIMESTONE	448.5	-	-	-	-	-
FG5-J	CHALKY LIMESTONE	448.5	-	-	-	-	-
FG5-K	CHALKY LIMESTONE	448.5	-	-	-	-	11
FG5-N	CHALKY LIMESTONE	462	-	-	-	-	-
FG5-P	CHALKY LIMESTONE	462	-	-	-	-	-
FG5-L	CHALKY LIMESTONE	462	2.3	40	-	3.04	-
FG5-R	CHALKY LIMESTONE	481	2.3	37	-	6.13	-

(continued on next page)

Table 1. (continued)

Borehole reference	Lithology	Depth (m)	Density	Porosity ϕ (%)	Permeability k at 0.1 MPa (mD)	UCS (MPa)	P^* (MPa)
FG5-X	CHALKY LIMESTONE	481	-	-	-	-	-
GEO7D-113B	DOLOSTONE	381.2	2.58	6.96	-	-	-
GEO7D-113C	DOLOSTONE	381.2	2.57	4.61	-	-	-
GEO7D-113D	DOLOSTONE	381.2	2.59	4.96	-	128	-
GEO7D-113E	DOLOSTONE	381.2	2.54	4.21	-	-	-
GEO7D-113F	DOLOSTONE	381.2	2.6	4.53	-	-	-
GEO7D-115A	DOLOMITIC TRANSITION ZONE	388.7	2.56	6.15	-	-	-
GEO7D-116A	DOLOMITIC TRANSITION ZONE	392.4	2.65	7.29	-	-	-
GEO7D-116B	DOLOMITIC TRANSITION ZONE	392.4	2.6	11.27	-	46.78	-
GEO7D-116C	DOLOMITIC TRANSITION ZONE	392.4	2.62	10.84	-	-	-
GEO7D-119A	SHALY VOLCANIC TRANSITION ZONE	406.3	2.62	5.45	22.55	83.82	-
GEO7D-120A	SHALY VOLCANIC TRANSITION ZONE	412.9	2.45	15.52	40.59	31.35	-
GEO7D-120C	SHALY VOLCANIC TRANSITION ZONE	412.9	2.47	13.39	-	-	-
GEO7D-120D	SHALY VOLCANIC TRANSITION ZONE	412.9	2.41	20.7	-	-	-
GEO7D-121A	SHALY VOLCANIC TRANSITION ZONE	416.9	2.35	18.82	24.21	-	-
GEO7D-121B	SHALY VOLCANIC TRANSITION ZONE	416.9	2.37	19.77	-	31.28	-
GEO7D-121C	SHALY VOLCANIC TRANSITION ZONE	417	2.51	13.18	-	-	-
GEO7D-130A	VOLCANISM	475	2.91	1.28	1.37	231.72	-
GEO7D-132A	VOLCANISM	485.7	2.75	1.96	0.26	-	-
GEO7D-132B	VOLCANISM	491.1	2.74	2.22	-	-	-
GEO7D-133A	VOLCANISM	501.6	2.5	10.62	-	-	-
GEO7D-135A	VOLCANISM	501.6	2.4	7.38	-	44.25	-
GEO7D-135B	VOLCANISM	513.9	2.4	11.95	-	-	-
GEO7D-138A	VOLCANISM	513.9	2.48	28.7	-	-	-
GEO7D-138B	VOLCANISM	513.9	2.46	33.55	-	-	-
GEO7D-138C	VOLCANISM	513.9	2.48	28.69	-	-	-
GEO7D-138D	VOLCANISM	513.9	2.45	28	156.54	16.78	-
GEO7D-160A	VOLCANISM	608	2.76	1.89	0.40	142.81	-
GEO7D-160B	VOLCANISM	608	2.78	1.8	-	-	-
GEO7D-160C	VOLCANISM	608	2.8	2.12	-	-	-
GEO7D-160D	VOLCANISM	608	2.78	1.95	-	-	-

Permeability is given in mD; 1 mD = 10^{-15} m². A strong disparity in density and porosity is observed within the basalts, which occur in three forms: a highly consolidated, dense and tightly porous form (porosity between 1 and 2%, sample 160B), a moderately porous form (around 10–12%, sample 135B) and a very altered form, which may be as porous as certain chalky limestones (porosity around 30%, sample 138A). Heterogeneity is also observed amongst the massive limestones (between 5 and 30% porosity, samples 35B vs. 50C) and in rocks of the clay-volcanic transition zone (between 5 and 20%, samples 119A, 120A and 121A). The upper limestones are not very competent and are associated with a disparity of densities ranging from 2.1 to a little more than 2.7 (Table 1). The porosity of these upper limestones is less than or equal to 10% for samples 2A and 31A, although certain levels of bio-constructed limestones reach total porosities between 20 and 28% (sample 23A). Contrary to other lithologies, indurated dolomites and rocks of the dolomitic transition zone show homogeneity in terms of porosity and density (between 4 and 10%, between 2.4 and 2.7, respectively—samples 107A to 116C).

Open porosity data have been collected using mercury porosimetry for several samples of chalky limestones (Figure 4). Each sample was divided in three sections for the measurements (except for

the sample GEO7D-104A). The pore distribution is heterogeneous depending on the cores, can be founded as unimodal for the only core sampled in borehole GEO7D (104A), trimodal (FG5-C and J)

Table 2. Permeability of the samples as a function of confining pressure (related to Figure 3b)

σ^3 (MPa)	Permeability of the samples (in mD)																		
	2A	38A	50C	66B	105B	106A	107A	109B	113A	116B	119A	120A	121A	130A	132A	135B	138D	160A	FG5
0.1	27.06	5.99	1.76	18.89	207.21	107.78	7.42	1.66	0.19	-	22.55	40.59	24.21	1.37	0.26	-	156.54	0.40	
0.2	30.20	1.59	0.44	26.27	198.81	141.95	1.27	0.61	0.04	-	18.06	40.25	21.42	0.78	0.15	6.68	154.67	0.23	
0.3	30.74	0.39	0.07	30.05	194.06	148.51	0.09	0.23	0.02	29.52	14.95	39.14	11.94	0.26	0.11	-	153.46	0.13	
0.4	30.77	0.11	0.04	30.87	193.60	147.37	-	0.18	0.01	-	13.86	38.53	6.95	0.09	0.06	0.38	152.53	0.067	
0.5	30.83	0.04	0.01	30.75	189.12	146.53	-	0.08	0.01	27.68	12.83	39.42	5.07	-	0.04	0.20	151.63	0.03	
0.6	-	0.01	-	-	-	-	-	0.041	-	-	-	-	-	-	0.032	0.02	-	0.03	
0.8	30.76	-	-	30.48	-	144.15	-	0.02	-	-	12.04	37.79	3.28	-	0.01	-	149.70	0.02	
1	30.8	-	-	30.37	182.75	142.15	-	0.01	-	18.15	11.83	37.14	2.94	-	0.01	-	148.39	0.01	
1.3	30.71	-	-	30.21	180.11	136.73	-	-	-	16.54	11.63	36.57	2.64	-	0.01	-	145.11	0.01	
2	30.51	-	-	30.10	175.15	127.27	-	-	-	15.51	11.39	35.11	2.51	-	-	-	139.20	-	
3	28.21	-	-	29.86	170.14	87.71	-	-	-	14.68	11.07	33.59	2.42	-	-	-	108.85	-	
4	24.15	-	-	28.56	162.29	61.38	-	-	-	13.26	10.75	32.32	2.37	-	-	-	92.47	-	
5	21.47	-	-	24.98	155.13	45.21	-	-	-	12.41	10.42	30.87	2.35	-	-	-	79.98	-	
10	11.54	-	-	13.51	138.19	14.29	-	-	-	5.68	7.71	2.27	-	-	-	63.03	-	-	
15	-	-	-	-	-	-	-	-	-	2.31	6.13	-	2.21	-	-	-	58.40	-	
20	-	-	-	-	-	-	-	-	-	1.22	5.34	-	2.17	-	-	-	-	-	
30	-	-	-	-	-	-	-	-	-	-	3.71	-	2.03	-	-	-	-	-	
40	-	-	-	-	-	-	-	-	-	-	2.44	-	2.02	-	-	-	-	-	

Permeability is given in mD; 1 mD = 10^{-15} m².

Table 3. Mercury porosimetry data related to the open porosities of the chalky limestones (related to Figure 4)

Borehole reference		Open porosity (%)	Pore throat diameter (μm)				Bulk density (g/mL)
GEO7D-104A	Top	54	40				1.41
	Middle	-	-				-
	Bottom	43	30				1.57
FG5-C	Top	35	14	4	0.55		1.59
	Middle	36	14	4	0.55		1.58
	Bottom	47	19	4	0.43		1.61
FG5-J	Top	41	19	3	0.43		2.02
	Middle	34	14	4	0.55		1.69
	Bottom	28	12	4	0.55		1.51
FG5-X	Top	40	40	19	4	0.34	1.57
	Middle	37	55	14	4	0.34	1.62
	Bottom	39	25	9	4	0.34	1.61

and quadrimodal (FG5-X) for samples sampled in the borehole FG5. This disparity can be explained by (i) the localization of the boreholes and (ii) the drilling period (2016 for GEO7D vs. 1980 for FG5 borehole, with the possibility of alteration over the

40 years of storage at CEA-DAM). The mean throat pore diameter of chalky limestones can be found at one of four mean ranges, depending on the geometry of the pore distribution. These ranges are 0.3–0.5 μm , 3–4 μm , 9–19 μm or 25–55 μm . This

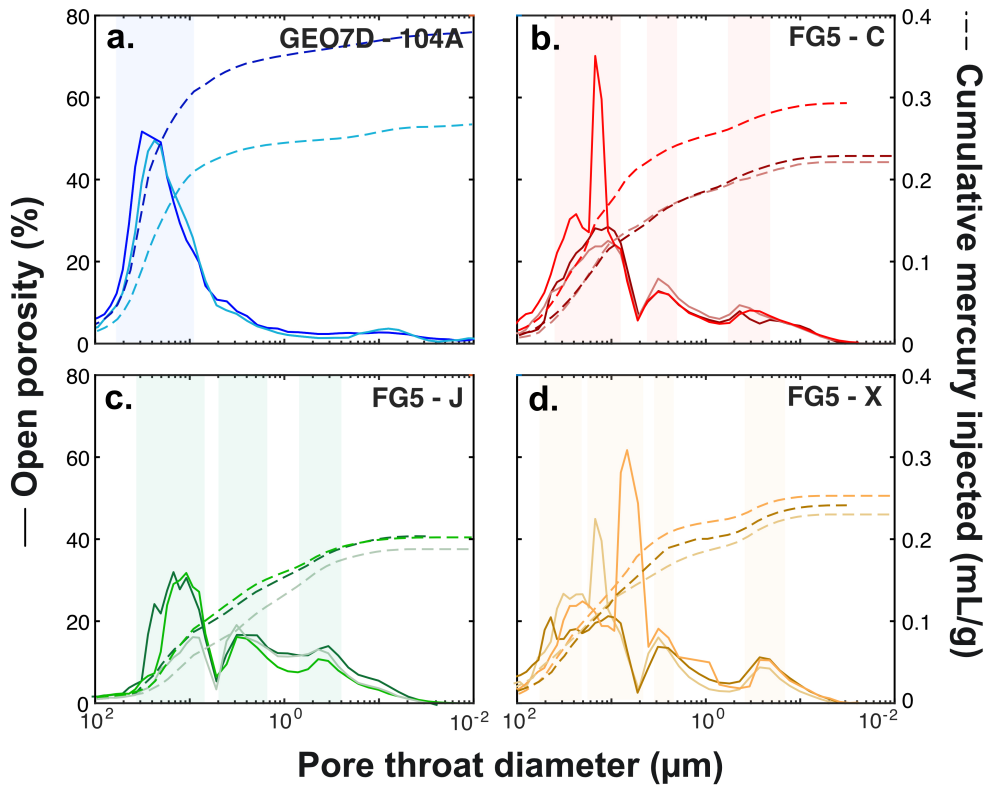


Figure 4. Pore throat diameter as a function of open porosity and cumulative mercury injected (in mL/g) for samples GEO7D-104 (a), and samples of the core FG5 (b–d). Each sample was divided in three sections (each curve—top, middle and bottom for the measurements).

heterogeneous pore distribution is explained by the particular and heterogeneous microstructure of chalky limestones.

The relationship between the evolution of permeability as a function of confining pressure is shown in Figure 3b. One can clearly distinguish two families:

- a first family that exhibits little pressure dependence (at least at pressures below the pore collapse pressure P^*), including chalky limestones, samples from the transition zone (samples 116B, 119A, 120A, 121A) as well as some massive and upper limestones (samples 2A and 66B). The permeability of these rocks is constant from 0 to 2 MPa, then abruptly decreasing above a critical pressure (P^*) which may be as low as 4 MPa (except for transition rocks for which a gradual decrease in permeability is observed at a lower value of 0.3 MPa—sample 121A).
- a second family for which permeability is strongly pressure dependent, including massive limestones, basalts excepting clayey and very altered basalts (as sample 138D) and indurated dolomites. For these rocks, the minimum permeability measurement threshold (approx. $1 \mu\text{d}$) attainable with our system was reached for confining pressures ranging between 0.4 and 1.3 MPa.

2.3.3. *A fine microstructure formed by equilibrium between mineralogy and marine bio-skeletons*

Chalky limestones are composed of calcite (CaCO_3), dolomite ($\text{CaMg}(\text{CO}_3)_2$) with some local traces of halite (NaCl). The grain size ranges from 10 to 100 μm . As shown by scanning electron micrographs prior to experiments (Figure 5a,b), chalky limestone is composed of planktonic skeletons (such as foraminifera and coccolithophores) and larger

marine organisms such as mollusks, echinoderms, or bryozoans. The presence of dolomite has been related to a dolomitization reaction during the history of atoll formation [Aissaoui *et al.*, 1986].

2.4. Sample preparation and experimental procedure for mechanical deformation

Cylindrical samples 40 mm in diameter and 80 mm in length were cored from selected samples from two boreholes (GEO7D and FG5) drilled at Mururoa (Figure 1). The samples were cut and drilled and then placed in a heat chamber at a temperature of 50 ± 2 °C for 72 h. Due to the high rate of breakage during drilling, only 23 out of more than 80 chalky limestone samples from the original cores were used for the experiments. These samples were taken from 7 in GEO7D core and 16 in FG5 core.

The samples were deformed at room temperature using a triaxial oil loading press [Laboratoire de Géologie de l'École Normale Supérieure, Paris, France; Aubry *et al.*, 2018, 2020, Fortin *et al.*, 2005, Schubnel *et al.*, 2007]. Ready for testing, the sample was placed in a 8 mm thick jacket (Viton Rubber FKM B, EFB75CS, Elastomer Engineering) to isolate it from the oil confining fluid. Strain gages were not used in the experiments. All initial tests resulted in strain gage breakages even when the pores in surface were filled with epoxy and polished to improve adhesion. Pore volume change was monitored using a micro-volumetric syringe pump (Quizix 10K, Laboratoire de Géologie de l'École Normale Supérieure, Paris, France), in order to observe the compaction of the rock on the water-saturated specimen only. Post-mortem specimens were impregnated with mounting resin and finally cut in half and polished for microstructural analysis.

Hydrostatic and deformation experiments were carried out according to a three-stage experimental plan:

- (a) Hydrostatic compression tests were performed on chalky limestones only (GEO7D and FG5 samples), under drained water saturated conditions, to determine the critical pore collapse pressure P^* . These experiments consisted of first saturating the chalk sample for 24 h and then gradually increasing the confining pressure up to 90 MPa (± 0.1 MPa) at a loading rate of 0.01 MPa/s.

The pore fluid pressure was constant at $9 \text{ MPa} \pm 0.05 \text{ MPa}$ —the maximum pore fluid pressure that can be applied to the Quizix pump—in all experiments except one which was carried out at $2 \text{ MPa} \pm 0.05 \text{ MPa}$. The compaction $\Delta V/V$ is measured during the experiments with the compressibility of grains being disregarded. Consequently, it is simply the change in porosity that is observed.

- (b) Triaxial deformation tests have been carried out on water-saturated chalky limestones (FG5 samples) at effective pressures between 2 and 10 MPa. These experiments consist of saturating the sample with water for 24 h at constant pore pressure, then deforming the sample at a constant axial deformation rate, at a constant pore pressure of 2 MPa (chosen for allowing us to perform long-time experiments without stopping or re-filling the Quizix pump in water before the end of the experiment). The axial shortening rate was fixed at $10 \text{ } \mu\text{m/s}$ (i.e. a strain rate of $10^{-5}/\text{s}$).
- (c) In addition, triaxial deformation tests were carried out on dry chalky limestones (FG5 samples), at confining pressures between 2 and 10 MPa to investigate possible water-related weakening. C^* was determined with stress–strain data.

3. Results: compaction and pore-collapse experiments

In the following, compressive stresses, shortening and volumetric compaction are considered positive. Compaction is denoted $\Delta V/V$. Axial and radial stresses are denoted σ_1 and σ_3 , respectively. The difference $\sigma_1 - \sigma_3$ is defined as the differential stress. The effective pressure P_{eff} , is defined as the difference between the confining pressure P_c and the pore fluid pressure P_p : $P_{\text{eff}} = P_c - \alpha P_p$ where α is the effective stress coefficient. The effective mean stress P_m is calculated as $(\sigma_1 + 2\sigma_3)/3 - P_p$.

3.1. Experiments under hydrostatic condition

The pore collapse of chalky limestone is studied according to three initial porosities (Figure 6a) and two

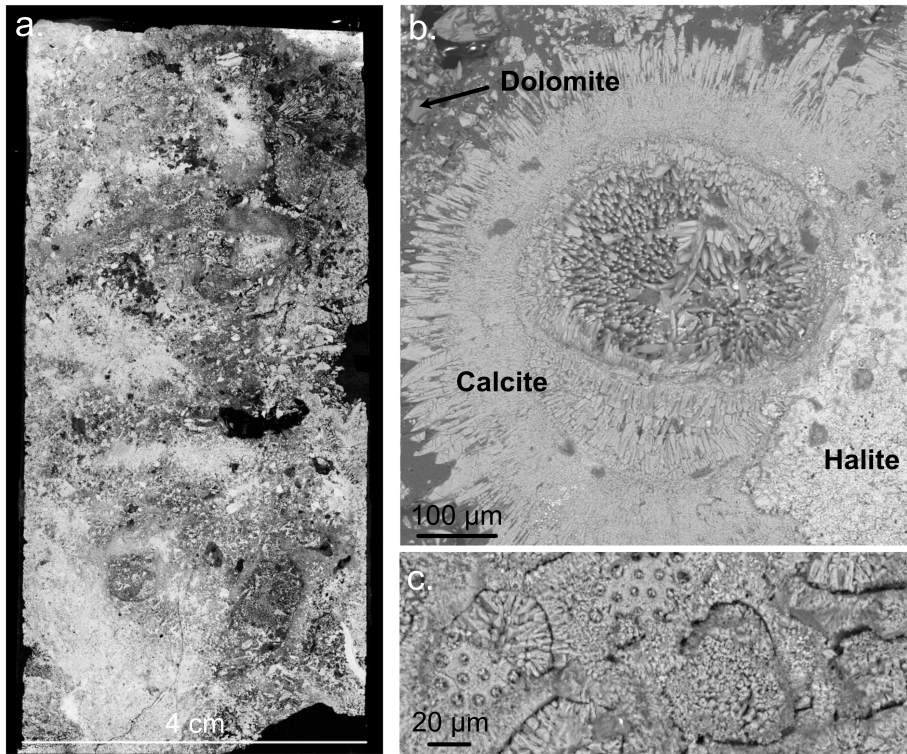


Figure 5. SEM micrographs and composition of chalky limestone. (a) SEM micrographs of a sample before the experiment. (b) Mineralogical composition of chalky limestones. (c) Bio-construction and marine fossil skeletons of the chalky limestone matrix.

different pore pressures (Figure 6b). Whatever their initial porosity (26, 38 and 42%), the critical pressure of pore collapse P^* was attained at effective pressure ranging between 16 and 18 MPa, i.e. pressures equivalent to an approximate depth of >1 km (assuming hydrostatic conditions and an average solid density of 2500 kg/m^3). Their initial porosity has an influence on the mechanical behavior for pressure higher than P^* . Figure 6b report two hydrostatic experiments performed on chalky limestones of the same porosity (40%), but at different pore pressure (at 2 or 9 MPa). For FG5 samples, P^* was reached at 11 and 14 MPa, for the experiments at pore pressures of 2 and 9 MPa, respectively—at lower P^* values than for GEO7D samples. Figure 6b shows that the evolution of $\Delta V/V$ during P_{eff} increase and the position of P^* were not affected to a great extent by the change in pore fluid pressure (meaning that α is close to 1).

3.2. Triaxial deformation experiments in water-saturated and dry conditions

During triaxial deformation, samples exhibit an elastic loading followed by shear-enhanced compaction at all the effective pressures tested (Figure 7). Compaction ranged from 3% at 2 MPa of effective pressure to almost 10% at 10 MPa of effective pressure. Above 6 MPa of effective pressure, compaction was associated with strain hardening (Figure 7—top), for axial deformation up to a maximum of 30%. Strain weakening was only observed at the effective pressure of 2 and 4 MPa. At 2 MPa of effective pressure, a few stress drops were associated with an acceleration of the volumetric strain or compaction—not at 4 MPa. In consequence, our mechanical investigation suggests that strain-weakening (i.e. stress release) may occur in chalky limestone, but below an effective pressure of 4 MPa (i.e. an approximate depth of 250 m, using the same assumptions as above).

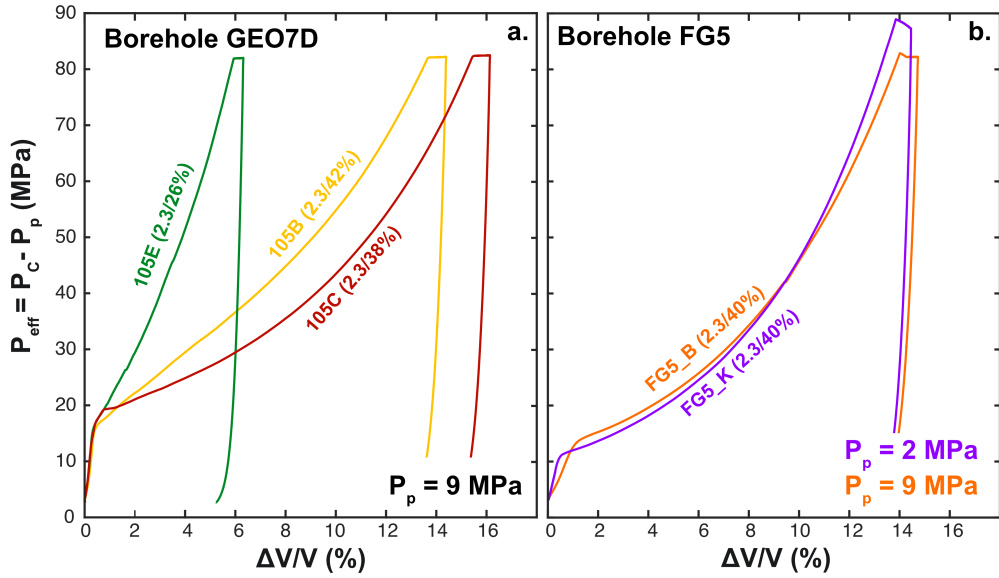


Figure 6. Effective pressure as a function of compaction. (a) For 3 chalky limestones from the GEO7D borehole with different porosities at a pore pressure of 9 MPa. (b) For two chalky limestones from the FG5 borehole at pore pressures of 2 and 9 MPa.

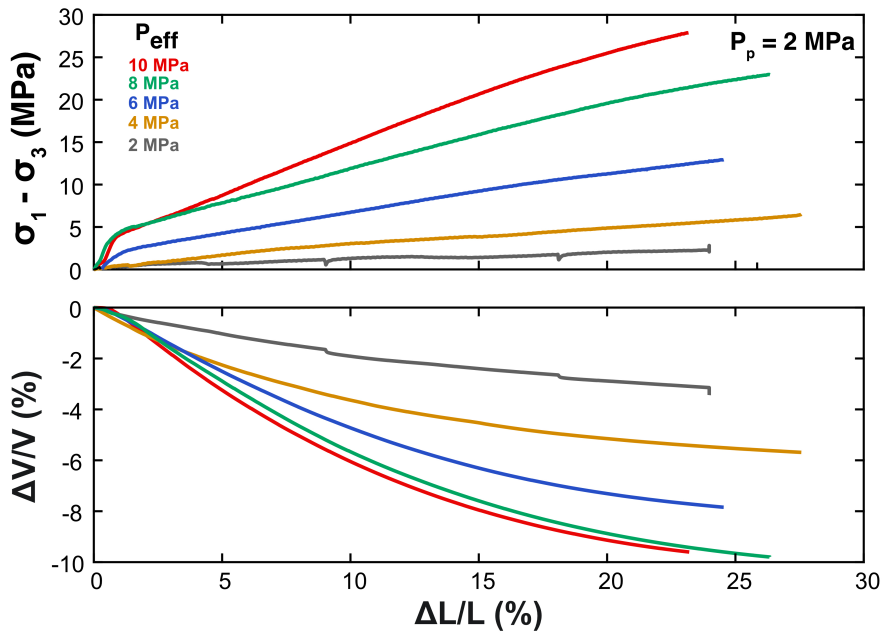


Figure 7. Mechanical data for water-saturated deformation tests. Differential stress and compaction as a function of axial deformation for water-saturated chalky limestones between 2 and 10 MPa (depending on color) at a constant pore pressure of 2 MPa.

Volumetric strain data are not available for the dry samples, as strain gages were not used in these

experiments. Overall, the mechanical data for the dry and wet experiments are qualitatively the

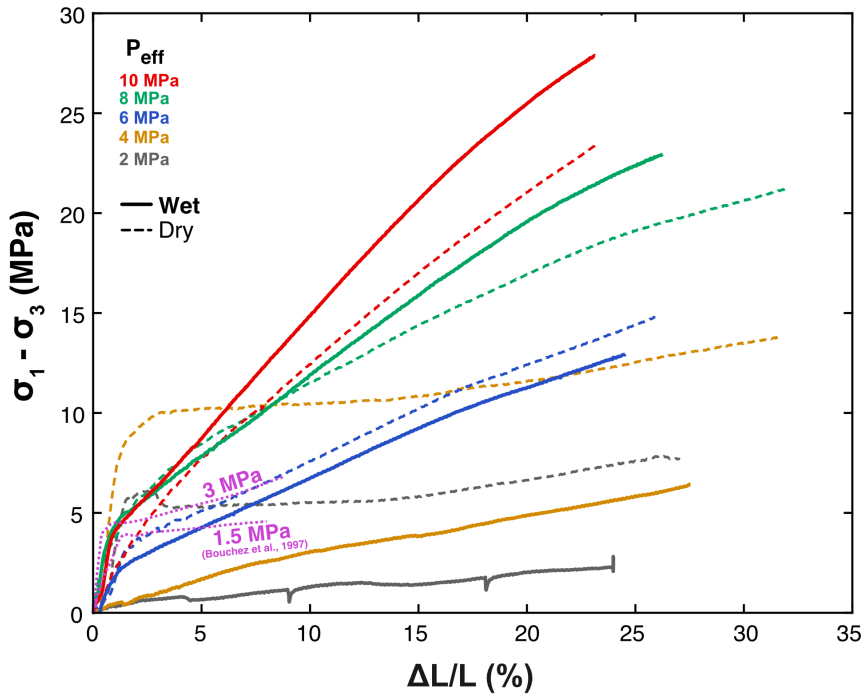


Figure 8. Compilation of water saturated and dry experiments. Differential stress as a function of axial deformation for water-saturated and dry chalky limestones between 2 and 10 MPa of effective pressure, in water-saturated and dry conditions (color and line thickness codes). The wet experiments were carried out at a pore pressure of 2 MPa. The mechanical data are compared with the only laboratory geomechanical data published to date on the Mururoa chalky limestones [in pink; Bouchez et al., 1997]—at low confining pressures (1.5 and 3 MPa) and at strain rates from 10^{-11} to 10^{-9} s $^{-1}$.

same. Yet, for effective pressure below 8 MPa the yield stresses appear largely reduced in the water-saturated experiments (Figure 8). Above 8 MPa of effective pressure, yield stresses are found to be in the same range than for dry experiments. In dry condition, a stress release appears to occur after the yield stress is reached during the experiment at 2 MPa, like in the water-saturated case.

3.3. Microstructures on post-mortem samples

Samples deformed under wet conditions were difficult to impregnate with epoxy resin, and are therefore not shown in the study. SEM micrographs of samples deformed at 2 and 10 MPa of confining pressure in dry conditions are shown in Figure 9. Scanning-electron micrographs of the sample deformed at 2 MPa effective pressure shows several areas of disaggregated and crushed material

(Figure 9a). At 10 MPa of effective pressure, deformation is enhanced by shear-enhanced compaction. The compaction is not homogeneous and seems to depend on the initial microstructure (Figure 9b).

4. Discussion–conclusion

The permeability measurements under confining pressure show two families of rocks (Figure 3), with the ease with which water can pass through depending, or not, at the depth of burial of the rock. This dichotomy can be explained by the structure and the initial micro-fracturing state of the different rocks: rocks with low permeability, or whose permeability is highly dependent on the confining pressure (Figure 3), appear as rocks with micro-fractures in a dense matrix with small grain size and low porosity. Permeable rocks, for which the permeability is not dependent on pressure, are the more

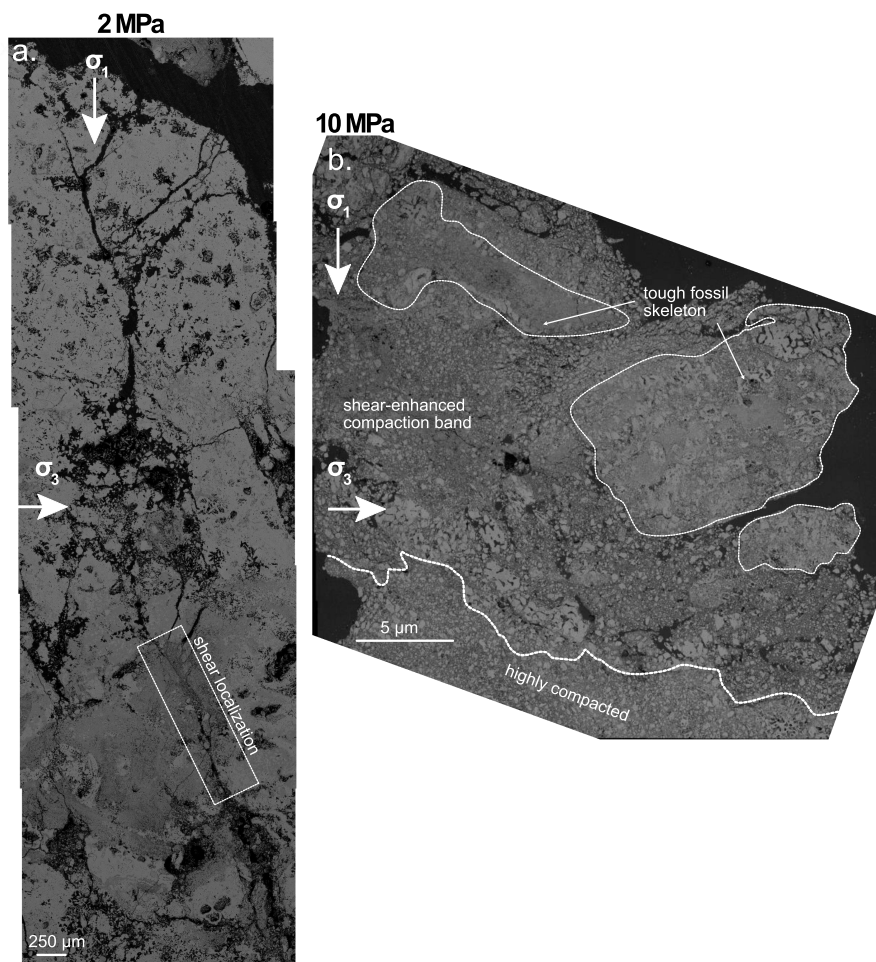


Figure 9. SEM on a sample deformed at 2 MPa (a) and 10 MPa (b) of confining pressure in dry condition.

porous rocks with numerous millimetric or micrometric voids and interstices, visible even on the surface of the sample. The fact that this second family of rocks does not show a permeability-pressure dependency means that the voids are connected. In the first family the connectivity is controlled by the microcracks which explain the pressure sensitivity [Vinciguerra *et al.*, 2005].

Initial porosity plays a role in the peak stress at failure in the brittle regime and for the onset of shear-enhanced compaction (Figure 10). Chalky limestones are porous, permeable and weak rocks with a high compaction capacity compared to results reported in the literature on other porous rocks (Figure 10), including chalks and limestones deformed in the laboratory under similar conditions [Baud *et al.*,

2009, 2017b, Geremia *et al.*, 2021, Xie *et al.*, 2011]. They appear to be compactant and mechanically unstable (Figures 2–5), with mechanical properties close to those of Obourg chalk [Geremia *et al.*, 2021; Figure 9] and P^* close to 16–18 MPa under water saturation (Figure 5). Under hydrostatic conditions, the influence of pore pressure seems slightly or just as important as the initial porosity (Figure 6a,b). The microstructural heterogeneity of chalky limestones can be explained by their deposition conditions, the variations in sea and phreatic levels [Fabricius, 2007] and the mechanical forcing and relative compaction induced by the past nuclear tests.

Within the atoll, water transfers between the lagoon and the ocean, and through the internal structure of the atoll, are influenced by a geothermal flux

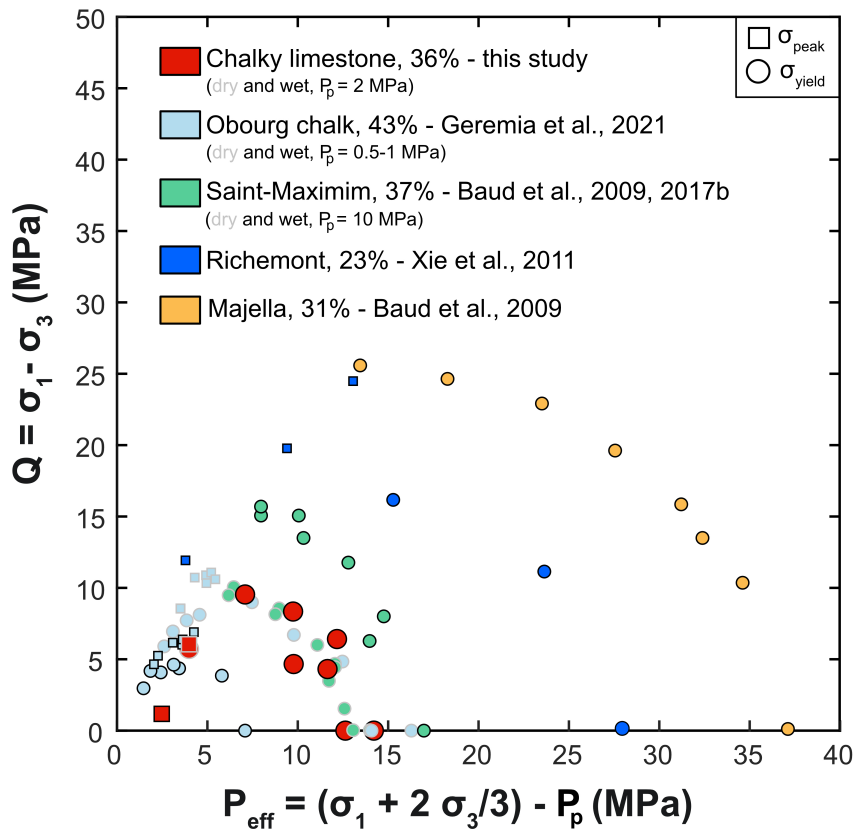


Figure 10. Comparison of the experimental results with a compilation of mechanical yield envelopes for chalky limestones and porous rocks with low critical pore collapse values.

[Rougerie and Wauthy, 1986], are conducive to fluid overpressures that affect the strength of less consolidated rocks, and facilitate localized gravity collapses or landslides [Keating and McGuire, 2000, Viesca and Rice, 2012]. In the context of a crown open to the ocean, karstified or poorly consolidated rocks are also affected by erosion, dissolution or hydrolytic alteration processes that contribute to their progressive weakening [Parise and Lollino, 2011]. The transient displacement measured in the north-east zone of the atoll could be explained by the localization of the deformation under the effect of a progressive compaction and a local hydrological forcing to overpressure in the most porous and permeable levels of the stratigraphic sequence, including in chalky limestones.

Although not directly dedicated to the study of the geomechanical deformation of atolls, several experi-

mental studies discuss the influence of water on the mechanical behavior for a better understanding of the petroleum reservoirs mechanics. These studies show that the weakening effect of water is associated to a decrease in Young's and bulk moduli, pore collapse yield stress and cohesion with increasing water saturation [Amour *et al.*, 2021, Foged *et al.*, 1996, Papamichos *et al.*, 1997, Risnes *et al.*, 1996, Schroeder and Shao, 1996]. Foged *et al.* [1996] also showed an increase in the rate of deformation with increasing initial water saturation.

In the brittle regime and in the presence of water (Figure 7), chalky limestones failed at low effective pressures (2 MPa). Failure occurs through microcracking and shear localization as in others lithologies referenced in the literature (Figure 10). The water-weakening effect can be explained by a reduction in surface energy and fracture toughness [Geremia

et al., 2021, Noël et al., 2024], dissolution and pressure solution [Newman, 1983], bond rupture at crack tips [Parks, 1984] and a reduction in capillary forces [i.e. between solid grain surface and water; Brignoli et al., 1994, Papamichos et al., 1997, Risnes and Flaage, 1999].

Above an effective pressure of 4 MPa, microcracking and pore collapse disappear in favor of hardening accommodated by shear-enhanced compaction and grain-crushing (Figure 8), except in some areas where the stiffer microfossil shells remain unaffected (Figure 9). Our experiments also show that water has no effect on compaction above an effective pressure of 6 MPa, indicating that the yield strength is almost the same for dry or wet experiments at higher effective pressures. This is consistent with the results reported by Nicolas et al. [2017] which showed a water weakening effect in the brittle regime of Tavel limestone (a rock with a porosity of 14%, less porous compared to chalky limestones), but no effect on the yield strength at the onset of compaction. Compared to the Obourg chalk [Geremia et al., 2021], no localization markers are found in the post-mortem water-saturated samples. This phenomenon can be attributed to the fact that water-saturated samples deformed by more than 20% of axial deformation are completely disaggregated, whatever the important structural heterogeneity of chalky limestones. In order to gain a more comprehensive understanding of this process, it would have been beneficial to conduct systematic microstructural analysis before and after the experiments, particularly with X-ray computed tomography.

In summary, chalky limestones exhibit a transition from microcracking at extremely low effective pressures to shear-enhanced compaction, associated with pore collapse and grain-crushing at higher effective pressures. This result, obtained after a substantial axial deformation, has significant implications for the long-term stability of the Mururoa atoll rim, as well as for the geomechanics of several other chalk environments.

Declaration of interest

The authors do not work for, advise, own, or receive funding from any organization that would benefit from this article, and have declared no affiliations other than their research organizations.

Funding

This work was supported by the LRC Yves Rocard (Laboratoire de Recherche Conventionné CEA-ENS-CNRS).

Acknowledgements

We thank J.-P. Avouac, P. Pras and A. Loevenbruck for fruitful discussions about the project. C. Lallemand and A. Loevenbruck help us in providing the samples drilled in Mururoa.

References

- Abadie, S. M., Harris, J. C., Grilli, S. T., and Fabre, R. (2012). Numerical modeling of tsunami waves generated by the flank collapse of the Cumbre Vieja Volcano (La Palma, Canary Islands): Tsunami source and near field effects. *J. Geophys. Res.: Ocean.*, 117(C5), article no. C05030.
- Aissaoui, D. M., Buigues, D., and Purser, B. H. (1986). Model of reef diagenesis: Mururoa atoll, French Polynesia. In *Reef Diagenesis*, pages 27–52. Springer, Berlin, Heidelberg.
- Al Heib, M., Duval, C., Theoleyre, F., Watelet, J. M., and Gombert, P. (2015). Analysis of the historical collapse of an abandoned underground chalk mine in 1961 in Clamart (Paris, France). *Bull. Eng. Geol. Environ.*, 74, 1001–1018.
- Amour, F., Christensen, H. F., Hajiabadi, M. R., and Nick, H. M. (2021). Effects of porosity and water saturation on the yield surface of Upper Cretaceous reservoir chalks from the Danish North Sea. *J. Geophys. Res.: Solid Earth*, 126(3), article no. e2020JB020608.
- Aubry, J., Passelègue, F. X., Deldicque, D., Girault, F., Marty, S., Lahfid, A., et al. (2018). Frictional heating processes and energy budget during laboratory earthquakes. *Geophys. Res. Lett.*, 45(22), 12–274.
- Aubry, J., Passelègue, F. X., Escartín, J., Gasc, J., Deldicque, D., and Schubnel, A. (2020). Fault stability across the seismogenic zone. *J. Geophys. Res.: Solid Earth*, 125(8), article no. e2020JB019670.
- Baud, P., Exner, U., Lommatzsch, M., Reuschlé, T., and Wong, T. F. (2017a). Mechanical behavior, failure mode, and transport properties in a porous carbonate. *J. Geophys. Res.: Solid Earth*, 122(9), 7363–7387.

- Baud, P., Klein, E., and Wong, T. F. (2004). Compaction localization in porous sandstones: spatial evolution of damage and acoustic emission activity. *J. Struct. Geol.*, 26(4), 603–624.
- Baud, P., Schubnel, A., Heap, M., and Rolland, A. (2017b). Inelastic compaction in high-porosity limestone monitored using acoustic emissions. *J. Geophys. Res.: Solid Earth*, 122(12), 9989–10008.
- Baud, P., Vinciguerra, S., David, C., Cavallo, A., Walker, E., and Reuschlé, T. (2009). Compaction and failure in high porosity carbonates: Mechanical data and microstructural observations. *Pure Appl. Geophys.*, 166, 869–898.
- Bouchez, J., Caristan, Y., and Mariotti, C. (1997). Stabilité des pentes sous-marines de l'atoll de Mururoa sous sollicitations dynamiques. *Rev. Fr. Géotech.*, (78), 3–13.
- Brignoli, M., Santarelli, F. J., and Righetti, C. (1994). Capillary phenomena in an impure chalk. In *SPE/ISRM Rock Mechanics in Petroleum Engineering*. SPE, Delft, Netherlands. (pp. SPE-28135).
- Brossard, J. and Duperret, A. (2004). Coastal chalk cliff erosion: experimental investigation on the role of marine factors. *Geol. Soc. Lond. Eng. Geol. Spec. Publ.*, 20(1), 109–120.
- Buigues, D., Gachon, A., and Guille, G. (1992). Mururoa atoll (French Polynesia). 1. Structure and geological evolution. *Bull. Soc. Géol. Fr.*, 163, 645–657.
- Castagna, A., Ougier-Simonin, A., Benson, P. M., Browning, J., Walker, R. J., Fazio, M., and Vinciguerra, S. (2018). Thermal damage and pore pressure effects of the Brittle–Ductile transition in Comiso limestone. *J. Geophys. Res.: Solid Earth*, 123(9), 7644–7660.
- CEA/DAM (2021). Surveillance des atolls de Moruroa et de Fangataufa. Tome II. Bilan géomécanique. CEA/DIF/DASE/SLDG/62/2021/DO.
- De Gennaro, V., Delage, P., Priol, G., Collin, F., and Cui, Y. J. (2004). On the collapse behaviour of oil reservoir chalk. *Géotechnique*, 54(6), 415–420.
- Duba, A. G., Abey, A. E., Bonner, B. P., Heard, H. C., and Schock, R. N. (1974). High-pressure mechanical properties of Kayenta sandstone. Technical Report UCRL–51526, California University, <https://www.osti.gov/servlets/purl/4327076>.
- Dunn, D. E., LaFountain, L. J., and Jackson, R. E. (1973). Porosity dependence and mechanism of brittle fracture in sandstones. *J. Geophys. Res.*, 78(14), 2403–2417.
- Duperret, A., Genter, A., Martinez, A., and Mortimore, R. N. (2004). Coastal chalk cliff instability in NW France: role of lithology, fracture pattern and rainfall. *Geol. Soc. Lond. Eng. Geol. Spec. Publ.*, 20(1), 33–55.
- Duperret, A., Genter, A., Mortimore, R. N., Delacourt, B., and De Pomerai, M. R. (2002). Coastal rock cliff erosion by collapse at Puys, France: the role of impervious marl seams within chalk of NW Europe. *J. Coast. Res.*, 18(1), 52–61. <https://www.jstor.org/stable/4299053>.
- El Khattabi, J., Carlier, E., and Louche, B. (2018). The effect of rock collapse on coastal cliff retreat along the chalk cliffs of Northern France. *J. Coast. Res.*, 34(1), 136–150.
- Fabricius, I. L. (2007). Chalk: composition, diagenesis and physical properties. *Bull. Geol. Soc. Denmark*, 55, 97–128. <http://2dgg.dk/publikationer/bulletin/index.html>.
- Fairhurst, C., Brown, E. T., Detournay, E., Marsily, G. D., Nikolaevshiy, V., Pearson, J. R., et al. (1999). *Underground Nuclear Testing in French Polynesia: Stability and Hydrology Issues*. International Geomechanical Commission, University of Minnesota, Minneapolis, Minnesota, <https://conservancy.umn.edu/handle/11299/162862>.
- Foged, N., Christensen, H. F., and Andersen, M. A. (1996). Rock mechanics and water injection. In *Proceedings of the 5th North Sea Chalk Symposium, Reims, France*.
- Fortin, J., Guéguen, Y., and Schubnel, A. (2007). Effects of pore collapse and grain crushing on ultrasonic velocities and Vp/Vs. *J. Geophys. Res.: Solid Earth*, 112(B8), article no. B08207.
- Fortin, J., Schubnel, A., and Guéguen, Y. (2005). Elastic wave velocities and permeability evolution during compaction of Bleurswiller sandstone. *Int. J. Rock Mech. Min. Sci.*, 42(7–8), 873–889.
- Fortin, J., Stanchits, S., Dresen, G., and Guéguen, Y. (2009). Acoustic emissions monitoring during inelastic deformation of porous sandstone: comparison of three modes of deformation. *Pure Appl. Geophys.*, 166(5), 823–841.
- Georgieva, T., Descamps, F., Gonze, N., Vandycke, S., Ajdanlijsky, G., and Tshibangu, J. P. (2020). Stability assessment of a shallow abandoned chalk mine of Malogne (Belgium). *Eur. J. Environ. Civil Eng.*, 27(6), 2358–2372.
- Geremia, D., David, C., Descamps, F., Menéndez, B.,

- Barnes, C., Vandycke, S., Dauriat, J., Esteban, L., and Sarout, J. (2021). Water-induced damage in microporous carbonate rock by low-pressure injection test. *Rock Mech. Rock Eng.*, 54(10), 5185–5206.
- Keating, B. H. and McGuire, W. J. (2000). Island edifice failures and associated tsunami hazards. *Pure Appl. Geophys.*, 157, 899–955.
- Keszthelyi, D., Dysthe, D. K., and Jamtveit, B. (2016). Compaction of North-sea chalk by pore-failure and pressure solution in a producing reservoir. *Front. Phys.*, 4, article no. 4.
- Lisabeth, H. P. and Zhu, W. (2015). Effect of temperature and pore fluid on the strength of porous limestone. *J. Geophys. Res.: Solid Earth*, 120(9), 6191–6208.
- McGuire, W. J. (2006). Lateral collapse and tsunami-genic potential of marine volcanoes. *Geol. Soc. Lond. Spec. Publ.*, 269(1), 121–140.
- McMurtry, G. M., Watts, P., Fryer, G. J., Smith, J. R., and Imamura, F. (2004). Giant landslides, megatsunamis, and paleo-sea level in the Hawaiian Islands. *Mar. Geol.*, 203(3–4), 219–233.
- Menéndez, B., Zhu, W., and Wong, T. F. (1996). Micromechanics of brittle faulting and cataclastic flow in Berea sandstone. *J. Struct. Geol.*, 18(1), 1–16.
- Montaggioni, L. F. (2005). History of Indo-Pacific coral reef systems since the last glaciation: development patterns and controlling factors. *Earth-Sci. Rev.*, 71(1–2), 1–75.
- Mortimore, R. N., Lawrence, J., Pope, D., Duperret, A., and Genter, A. (2004). Coastal cliff geohazards in weak rock: the UK Chalk cliffs of Sussex. *Geol. Soc. Lond. Eng. Geol. Spec. Publ.*, 20(1), 3–31.
- Newman, G. H. (1983). The effect of water chemistry on the laboratory compression and permeability characteristics of some North Sea chalks. *J. Pet. Technol.*, 35(5), 976–980.
- Nicolas, A., Fortin, J., Regnet, J. B., Dimanov, A., and Guéguen, Y. (2016). Brittle and semi-brittle behaviours of a carbonate rock: influence of water and temperature. *Geophys. J. Int.*, 206(1), 438–456.
- Nicolas, A., Fortin, J., Regnet, J. B., Verberne, B. A., Plümper, O., Dimanov, A., et al. (2017). Brittle and semibrittle creep of Tavel limestone deformed at room temperature. *J. Geophys. Res.: Solid Earth*, 122(6), 4436–4459.
- Noël, C., Fryer, B., Baud, P., and Violay, M. (2024). Water weakening and the compressive brittle strength of carbonates: Influence of fracture toughness and static friction. *Int. J. Rock Mech. Min. Sci.*, 177, article no. 105736.
- Papamichos, E., Brignoli, M., and Santarelli, F. J. (1997). An experimental and theoretical study of a partially saturated collapsible rock. Mechanics of Cohesive-frictional materials. *Int. J. Exp. Model. Comput. Mater. Struct.*, 2(3), 251–278.
- Parise, M. and Lollino, P. (2011). A preliminary analysis of failure mechanisms in karst and man-made underground caves in Southern Italy. *Geomorphology*, 134(1–2), 132–143.
- Parks, G. A. (1984). Surface and interfacial free energies of quartz. *J. Geophys. Res.: Solid Earth*, 89(B6), 3997–4008.
- Perrin, C. (1990). Genèse de la morphologie des atolls: le cas de Mururoa. *C. R. Acad. Sci. Paris*, 311(11), 671–678. <https://mnhn.hal.science/mnhn-02866800/>.
- Poupardin, A., Heinrich, P., Frère, A., Imbert, D., Hébert, H., and Flouzat, M. (2017). The 1979 submarine landslide-generated tsunami in Mururoa, French Polynesia. *Pure Appl. Geophys.*, 174(8), 3293–3311.
- Renaud, V., Cherkaoui, A., Watelet, J. M., and Gombert, P. (2019). Instability mechanisms of chalk mines in presence of water: feedback from the collapse of the Baulieu mine (France). In *1st International Symposium on Computational and Geoenvironmental Geomechanics for Underground and Subsurface Structure (COGGUS2)*. <https://ineris.hal.science/ineris-03319915/>.
- Risnes, R. and Flaageng, O. (1999). Mechanical properties of chalk with emphasis on chalk-fluid interactions and micromechanical aspects. *Oil Gas Sci. Technol.*, 54(6), 751–758.
- Risnes, R., Gjesdal, S. A., Landaas, T. L., and Madland, I. (1994). Changes in mechanical properties of chalk caused by deformation and by pore pressure. In *Proceedings of Eurock '94*. Balkema, Rotterdam.
- Risnes, R., Kristensen, C. N., and Andersen, M. A. (1996). Triaxial tests on high porosity chalk with different saturating fluids. In *Fifth North Sea Chalk Symposium, Reimes, France*, page 12.
- Rougerie, F. and Wauthy, B. (1986). Le concept d'endo-upwelling dans le fonctionnement des atolls-oasis. *Ocean. Acta*, 9(2), 133–148. <https://archimer.ifremer.fr/doc/00110/22126/19762.pdf>.
- Rowberry, M., Klimeš, J., Blahůt, J., Balek, J., and

- Kusák, M. (2023). A global database of giant landslides on volcanic islands. In *Progress in Landslide Research and Technology*, volume 1(1), pages 295–304. Springer International Publishing, Cham.
- Schock, R. N., Heard, H. C., and Stephens, D. R. (1973). Stress-strain behavior of a granodiorite and two graywackes on compression to 20 kilobars. *J. Geophys. Res.*, 78(26), 5922–5941.
- Schroeder, C. and Shao, J. (1996). Plastic deformation and capillary effects in chalks. In *5th North Sea Chalk Symposium*, pages 1–14. <https://onepetro.org/ISRMEUROCK/proceedings-abstract/EUROCK96/All-EUROCK96/ISRM-EUROCK-1996-160/50909>.
- Schubnel, A., Thompson, B. D., Fortin, J., Guéguen, Y., and Young, R. P. (2007). Fluid-induced rupture experiment on Fontainebleau sandstone: Premonitory activity, rupture propagation, and aftershocks. *Geophys. Res. Lett.*, 34(19), article no. L19307.
- Senfaute, G., Duperret, A., and Lawrence, J. A. (2009). Micro-seismic precursory cracks prior to rock-fall on coastal chalk cliffs: a case study at Mesnil-Val, Normandie, NW France. *Nat. Hazards Earth Syst. Sci.*, 9(5), 1625–1641.
- Sulak, R. M. (1991). Ekofisk field: the first 20 years. *J. Pet. Technol.*, 43(10), 1265–1271.
- Tembe, S., Baud, P., and Wong, T. F. (2008). Stress conditions for the propagation of discrete compaction bands in porous sandstone. *J. Geophys. Res.: Solid Earth*, 113(B9), article no. B09409.
- Vajdova, V., Baud, P., and Wong, T. F. (2004). Compaction, dilatancy, and failure in porous carbonate rocks. *J. Geophys. Res.: Solid Earth*, 109(B5), article no. B05204.
- Viesca, R. C. and Rice, J. R. (2012). Nucleation of slip-weakening rupture instability in landslides by localized increase of pore pressure. *J. Geophys. Res.: Solid Earth*, 117(B3), article no. B03104.
- Vinciguerra, S., Trovato, C., Meredith, P. G., and Benson, P. M. (2005). Relating seismic velocities, thermal cracking and permeability in Mt. Etna and Iceland basalts. *Int. J. Rock Mech. Min. Sci.*, 42(7–8), 900–910.
- Ward, S. N. and Day, S. (2001). Cumbre Vieja volcano—potential collapse and tsunami at La Palma, Canary Islands. *Geophys. Res. Lett.*, 28(17), 3397–3400.
- Wong, T. F. and Baud, P. (1999). Mechanical compaction of porous sandstone. *Oil Gas Sci. Technol.*, 54(6), 715–727.
- Wong, T. F. and Baud, P. (2012). The brittle-ductile transition in porous rock: A review. *J. Struct. Geol.*, 44, 25–53.
- Wong, T. F., Baud, P., and Klein, E. (2001). Localized failure modes in a compactant porous rock. *Geophys. Res. Lett.*, 28(13), 2521–2524.
- Wong, T. F., David, C., and Menendez, B. (2004). Mechanical compaction. *Int. Geophys. Ser.*, 89, 55–114. <https://hal.science/hal-03475852/document>.
- Wong, T. F., Szeto, H., and Zhang, J. (1992). Effect of loading path and porosity on the failure mode of porous rocks. *Appl. Mech. Rev.*, 45(8), 281–293.
- Wright, S. G. and Rathje, E. M. (2003). Triggering mechanisms of slope instability and their relationship to earthquakes and tsunamis. *Pure Appl. Geophys.*, 160, 1865–1877.
- Xie, S. Y., Shao, J. F., and Xu, W. Y. (2011). Influences of chemical degradation on mechanical behaviour of a limestone. *Int. J. Rock Mech. Min. Sci.*, 48(5), 741–747.
- Zaman, M., Roegiers, J. C., Abdulraheem, A., and Azeemuddin, M. (1994). Pore collapse in weakly cemented and porous rocks. *J. Energy Resour. Technol.*, 116(2), 97–103.
- Zhang, J., Wong, T. F., and Davis, D. M. (1990). Micromechanics of pressure-induced grain crushing in porous rocks. *J. Geophys. Res.: Solid Earth*, 95(B1), 341–352.
- Zhu, W., Baud, P., and Wong, T. F. (2010). Micromechanics of cataclastic pore collapse in limestone. *J. Geophys. Res.: Solid Earth*, 115(B4), article no. B04405.